

Skyrmion Control of Majorana States in Planar Josephson Junctions

Narayan Mohanta,¹ Satoshi Okamoto,¹ and Elbio Dagotto^{1,2}

¹*Materials Science and Technology Division, Oak Ridge National Laboratory, Oak Ridge, TN 37831, USA*

²*Department of Physics and Astronomy, The University of Tennessee, Knoxville, TN 37996, USA*

Planar Josephson junctions provide a versatile platform, alternative to the nanowire-based geometry, for the generation of the Majorana bound states (MBS), due to the additional phase tunability of the topological superconductivity. The proximity induction of chiral magnetism and superconductivity in a two-dimensional electron gas showed remarkable promises to manipulate topological superconductivity. Here, we propose a new device geometry involving a skyrmion crystal that resolves several issues of the planar Josephson junction and show that the MBS can be created and controlled using the skyrmions. The spin-orbit coupling generated by the skyrmions removes the requirement of a strong intrinsic Rashba spin-orbit coupling, and the phase biasing of the Josephson junction to realize the MBS. The skyrmion radius, being externally tunable by a magnetic field or an anisotropy, offers a useful control knob for the emergence of the MBS.

The unification of non-trivial spin texture and superconductivity via advanced interface engineering is a futuristic way to create and manipulate non-Abelian MBS for their controlled usage in fault-tolerant topological quantum computing¹⁻⁵. The nanoscale control of magnetism not only relaxes the need for a specific form of Rashba spin-orbit coupling (SOC), but also motivates for a magnetic field-free platform for the braiding of the MBS⁶⁻¹⁰. Despite numerous successes in the search for the MBS in one-dimensional geometries, the associated limitations such as the intrinsic instabilities of one-dimensional systems, the need for fine tuning of parameters, and the technological obstacles in physical implementation, suggest to look for a two-dimensional platform^{11,12}. The recent discovery of topological superconductivity in phase-controlled planar Josephson junctions (JJs) is, therefore, a major step towards the realization of a two-dimensional array of MBS for designing scalable braiding protocols¹³⁻¹⁵. The previous works on the JJ-based platforms, however, revealed the necessity of a strong intrinsic Rashba SOC and π -phase biasing of the JJ. Recently, a heterostructure involving a superconductor and a chiral magnet was proposed for topological superconductivity^{16,17}; but the location of the Majorana

states, in this platform, is difficult to anticipate due to their non-localized character.

In our considered geometry, the planar JJ, composed of a two-dimensional electron gas (2DEG) and an *s*-wave superconductor, is placed on top of a Néel-type skyrmion crystal (SkX) in such a way that the 2DEG experiences the spatially-varying magnetic field from the bottom SkX and it is also proximitized to the electron pairing from the top superconductors, as described in Fig. 1a. The interplay between the SkX spin texture and the proximity-induced superconductivity leads to topological superconductivity near the middle quasi-one-dimensional channel of the JJ with localized MBS at its two ends. The advantages of using the SkX are: (i) the chiral magnetism generates a SOC and a local Zeeman field which remove the stringent criteria of a strong Rashba-type SOC and, therefore, essentially expands the region of parameter space to realize the MBS, (ii) the existence of the MBS can be further controlled externally by tuning the skyrmion radius, and (iii) usual planar JJs are required to be phase biased with a phase difference $\varphi = \pi$, between the two superconducting regions, to minimize the critical magnetic field for the topological transition and to maximize the chemical-potential range within which the MBS appear¹³; the current SkX-based JJ is not required to be phase biased and the MBS can be found robustly at $\varphi = 0$. Using the zero-energy feature of the quasiparticle states with a topological energy gap, sharp localization of these states, charge-neutrality condition, two order parameters, *viz.* Majorana polarization and curvature of the density of states, we confirm the existence of the MBS in our set up.

For the generation of the SkX, we consider a heterostructure of a thin-layer ferromagnet (FM) and a heavy metal or a heavy insulator (HM/HI). The strong SOC in the HM/HI gives rise to a large Dzyaloshinskii-Moriya interaction (DMI) at the interface between the FM and the HM/HL. The cooperation between the DMI and the ferromagnetic exchange interaction of the FM produces a triangular SkX, in the presence of a magnetic field or an anisotropy. Our Monte Carlo simulations reveal that columns of skyrmions, arranged in a triangular array, appear spontaneously within a six-layer FM, although the DMI exists predominantly at the interface between

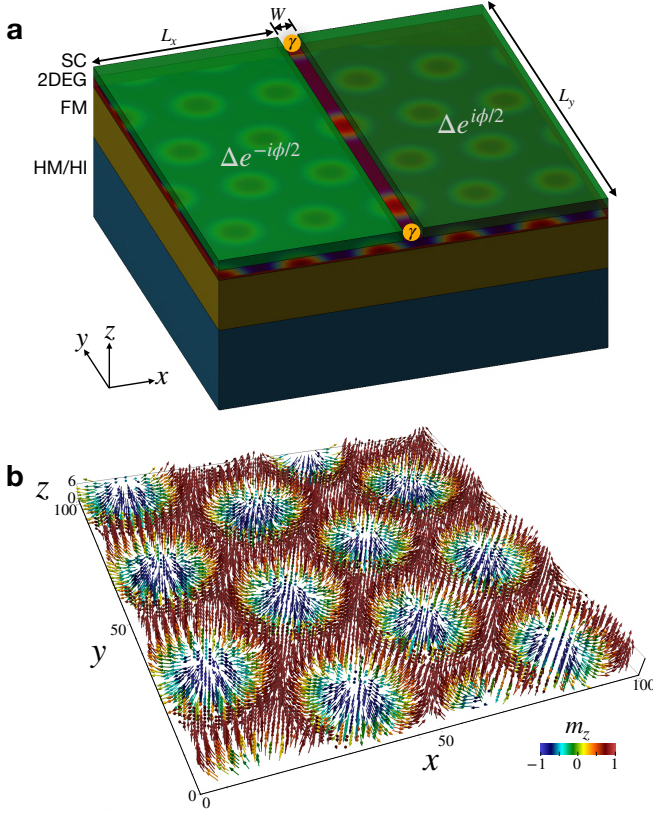


FIG. 1. **Device geometry and a skyrmion crystal.** **a.** Planar Josephson junction on top of a skyrmion crystal (SkX). The two-dimensional electron gas (2DEG) exhibits both proximity-induced superconductivity from the top superconductor (SC) layers and spatially-varying magnetism from the bottom SkX. The SkX is spontaneously created in the ferromagnet (FM) due to the competition between exchange interactions in the FM and the heavy metal or heavy insulator (HM/HI), with a field or anisotropy. The zero-energy Majorana bound states (yellow bubbles) are localized at the two ends of the quasi-one-dimensional metallic channel. **b.** The SkX spin texture, spontaneously generated in a Monte Carlo simulation using a $100 \times 100 \times 6$ lattice with ferromagnetic exchange interaction strength $J = 1$, DMI strength $D = 0.3J$, magnetic field $H_z = 0.1J$, spin amplitude $S = 1$, and easy-plane anisotropy $A = 0.01J$.

the FM and the HM/HI, as shown in Fig. 1b. We use Metropolis energy minimization technique (Supplementary Information SI.1) formulated with the following Hamiltonian

$$\begin{aligned} \mathcal{H} = & -J \sum_{\langle ij \rangle} \mathbf{S}_i \cdot \mathbf{S}_j - D \sum_{\langle ab \rangle} (\hat{z} \times \hat{r}_{ab}) \cdot (\mathbf{S}_a \times \mathbf{S}_b) \\ & - H_z \sum_i S_{zi} - A \sum_a |S_{za}|^2, \end{aligned} \quad (1)$$

where J is the nearest-neighbor ferromagnetic exchange interaction strength in the FM, D is the DMI strength at the bottom FM layer that interfaces with the HM/HI, H_z is the perpendicular magnetic field, A is the easy-plane magnetic anisotropy at the bottom FM layer, i, j are the site indices in the entire FM, and a, b are the

two-dimensional site indices at the bottom FM layer. The DMI, present dominantly at the interface between the FM and the HM/HI, generates a Néel-type SkX¹⁸. Besides the engineered interfaces, the SkX naturally appears in a wide variety of materials such as non-centrosymmetric magnets^{19–21} that can also be utilized in the proposed device geometry, instead of the combination of the FM and the HM/HI. Also, the SkX can be artificially-created without the need for any external magnetic field by nanopatternization²².

The spin texture \mathbf{B}_i on the top layer of the FM, obtained from the Monte Carlo simulations, is used to obtain the low-energy spectrum of the planar JJ by solving self-consistently the Bogoliubov-de Gennes equations (Supplementary Information SI.2). The proximity-induced superconductivity in the 2DEG, which is subject to the SkX spin texture \mathbf{B}_i , is described by the Hamiltonian

$$\begin{aligned} \mathcal{H}_{\text{BdG}} = & -t \sum_{\langle ij \rangle, \sigma} (c_{i\sigma}^\dagger c_{j\sigma} + H.c.) + \sum_{i, \sigma} (4t - \mu) c_{i\sigma}^\dagger c_{i\sigma} \\ & - \frac{1}{2} g \mu_B \sum_{i, \sigma} (\mathbf{B}_i \cdot \boldsymbol{\sigma})_{\sigma\sigma'} c_{i\sigma}^\dagger c_{i\sigma'} + \sum_i (\Delta_i c_{i\uparrow}^\dagger c_{i\downarrow}^\dagger + H.c.), \end{aligned} \quad (2)$$

where $t = \hbar^2 / (2m^*a^2)$ is the hopping energy, m^* is the effective mass of electrons, a is the unit spacing of the lattice grid, μ is the chemical potential, and Δ_i is the induced local s -wave pairing amplitude on the two sides of the JJ that are attached to the top Al layer. The pairing amplitude $\Delta_i = -U_i \langle c_{i\uparrow} c_{i\downarrow} \rangle$ is calculated self-consistently using the onsite attractive interaction strength U_i of the induced superconducting states in the 2DEG. $U_i = U$ in the 2DEG below the Al superconductors and zero in the middle metallic channel. The value $U = 2$ meV is determined by setting $\Delta_i = 0.2$ meV, the estimated proximity-induced gap magnitude for a 2DEG with an SC interface^{23,24}, without any spin texture. The g factor and the effective mass are set to $g = 50$ and $m^* = 0.017m_0$ for InSb^{25,26}. The lattice grid spacing used is $a = 10$ nm²⁷ with which the hopping energy becomes $t = 22.44$ meV. The amplitude of the spin texture \mathbf{B}_i is set to $B_0 = 0.3$ T, compatible with the saturation magnetization $M_s = 1.7 \times 10^6$ A/m for CoFe^{8,9}. We present results for a planar JJ with length $L_y = 2$ μm , transverse length of the SC leads $L_x = 200$ nm, and width of the quasi-one-dimensional metallic channel $W = 50$ nm.

The low-energy spectrum, shown in Fig. 2a, reveals that there exist multiple ranges of the chemical potential within which the zero-energy MBS appear. To determine the Majorana character of the quasiparticle states, we compute the Majorana polarization, defined as⁵

$$\mathcal{P}_{\mathcal{M}, n} = 2 \sum_i |u_{i\downarrow}^n v_{i\downarrow}^{n*} - u_{i\uparrow}^n v_{i\uparrow}^{n*}|, \quad (3)$$

where $u_{i\uparrow}^n$ and $v_{i\uparrow}^n$ are the Bogoliubov-de Gennes quasiparticle and quasihole amplitudes, respectively, corresponding to the n^{th} eigenstate, spin \uparrow , and site i . As evident from Fig. 2a, $\mathcal{P}_{\mathcal{M}, n} \gtrsim 1$ indicates the occurrence

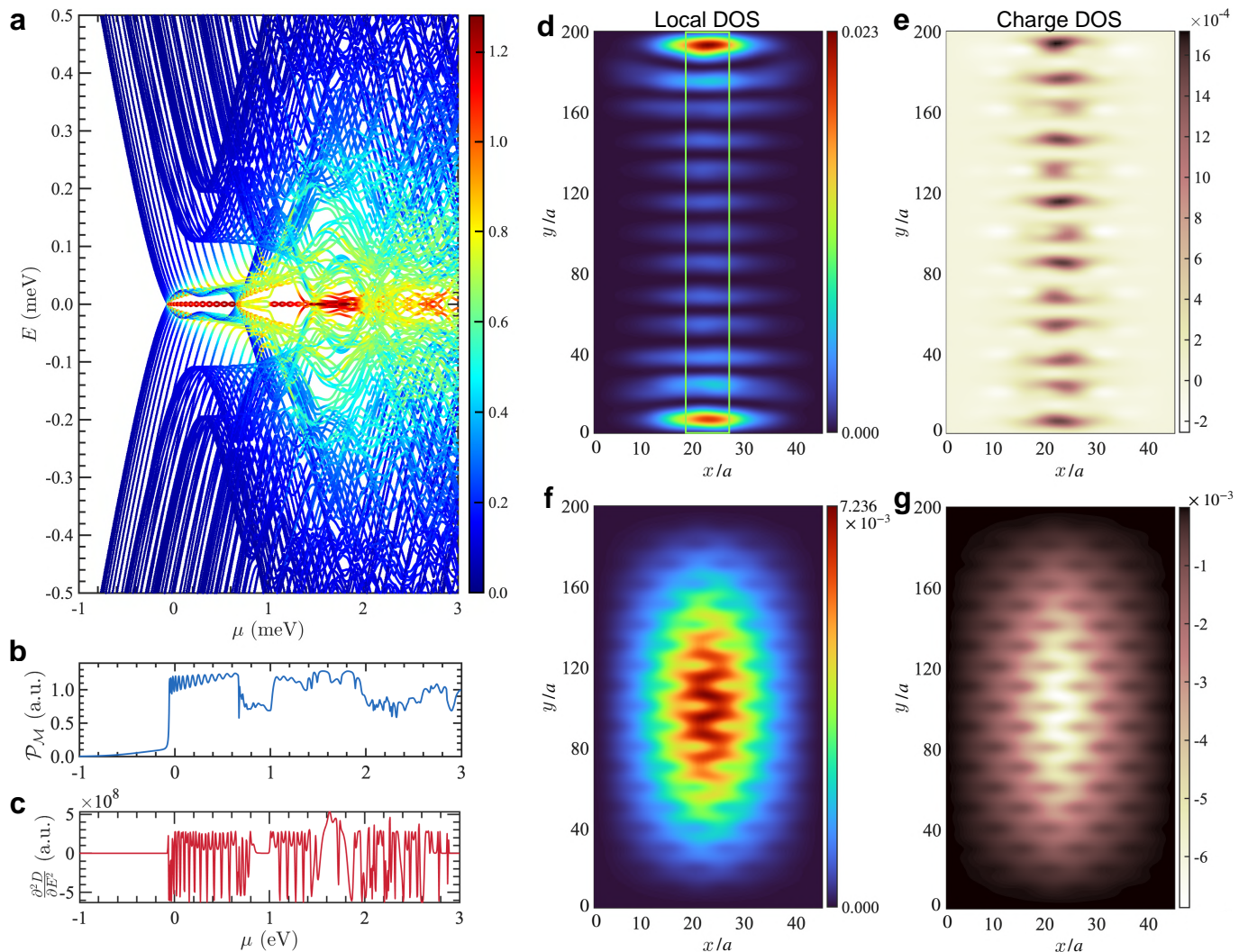


FIG. 2. **Emergence of the Majorana bound states with changing chemical potential.** **a.** The quasiparticle spectrum of the planar Josephson junction at phase difference $\varphi = 0$ with varying chemical potential (μ), showing the emergence of the zero-energy MBS. The colorbar represents the Majorana polarization \mathcal{P}_M that displays the Majorana character of the quasiparticle states. The SkX with a skyrmion diameter $D_{sk} = 10a$ was obtained using a magnetic field $H_z = 0.95J$ and a DMI strength $D = 1.6J$ in the Monte Carlo calculations. **b.**, **c.** The Majorana polarization \mathcal{P}_M and the curvature of the density of states at zero energy $\frac{\partial^2 D}{\partial E^2}$, with varying μ , showing the μ range within which the MBS appear. The delta-function-like peaks are associated with the oscillations of the MBS with changing μ . **d.** **e.** The profiles of the local density of states and the charge density of states at $\mu = 0.5$ meV. The green rectangle in **d** indicates the quasi-one-dimensional metallic channel of the planar Josephson junction at the ends of which the MBS appear. **f.**, **g.** The profiles of the local density of states and the charge density of states at $\mu = -0.5$ meV, in the non-topological regime.

of robust MBS with a finite topological energy gap (Supplementary Information SIV). The Majorana polarization \mathcal{P}_M , plotted with μ in Fig. 2b, acquires finite values within the range of μ , in which the MBS emerge. The delta function-like peaks in \mathcal{P}_M are the signatures of the Majorana oscillations, which is also clearly seen in the low-energy spectrum in Fig. 2a, originating due to the overlap of the MBS wave functions at the two ends of the finite-length quasi-one-dimensional channel. The Majorana oscillations in \mathcal{P}_M have also been confirmed from the calculations of a one-dimensional wire (Supplementary Information SII). To further characterize the evolu-

tion of the topological superconductivity with changing a parameter, such as μ , we look at the curvature of the density of states at zero energy $\frac{\partial^2 D}{\partial E^2}$, where $D(E)$ is defined as⁷

$$D(E) = \sum_{i,n,\sigma} (|u_{i\sigma}^n|^2 + |v_{i\sigma}^n|^2) \delta(E - E_n), \quad (4)$$

and $\delta(E - E_n)$ is modeled using a Gaussian with broadening 0.001 meV ($\ll t$). The second derivative is computed using the second-order finite-difference method. As shown in Fig. 2c, $\frac{\partial^2 D}{\partial E^2}$ takes finite values in the same ranges of μ as that of the Majorana polarization \mathcal{P}_M .

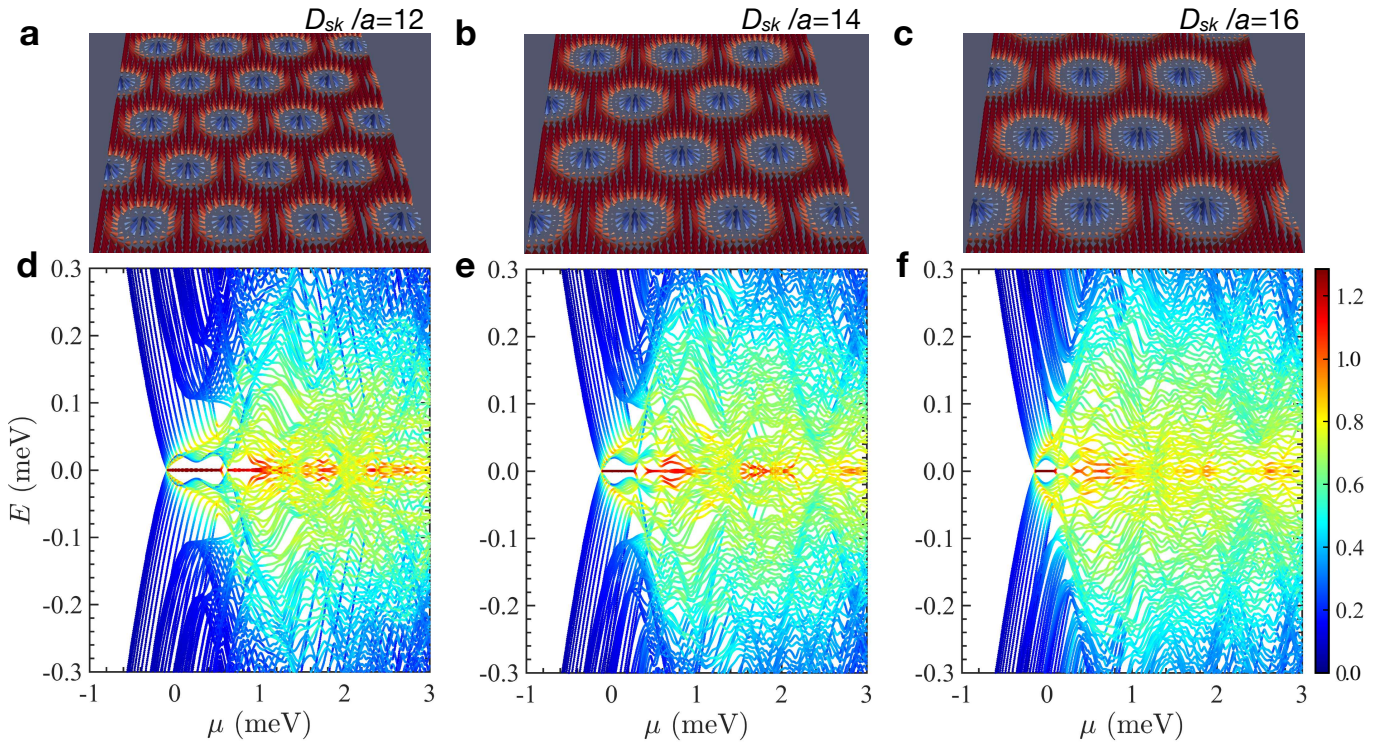


FIG. 3. **Skyrmion tuning of the Majorana bound states.** **a-c** The skyrmion crystals of different skyrmion diameters **a.** $D_{sk} = 12a$, **b.** $D_{sk} = 14a$, **c.** $D_{sk} = 16a$, obtained in the Monte Carlo calculations using **a.** a magnetic field $H_z = 0.8J$, a DMI strength $D = 1.4J$, **b.** $H_z = 0.45J$, $D = J$, and **c.** $H_z = 0.23J$, $D = 0.6J$. **d-f** The corresponding quasiparticle spectra of the planar Josephson junction at the phase difference $\varphi = 0$ with varying chemical potential, obtained by solving the Bogoliubov-de Gennes equations with the above skyrmion crystal spin configurations. The colorbar in **d-f** represents the Majorana polarization \mathcal{P}_M of the quasiparticle states.

The Majorana oscillations, in the form of delta-function-like peaks, is also noticeable in $\frac{\partial^2 D}{\partial E^2}$, albeit with changes in the sign. To visualize the location of the zero-energy MBS, we show, in Fig. 2d, the profile of the local density of states $\rho_{\text{LDOS}}^i = \sum_{\sigma} (|u_{i\sigma}|^2 + |v_{i\sigma}|^2)$, corresponding to the lowest positive-energy eigenstate at $\mu = 0.5$ meV where the JJ is in the topological superconducting regime. The sharp peaks in ρ_{LDOS}^i indicate that the MBS are localized predominantly near the two ends of the quasi-one-dimensional channel. Figure 2e shows the profile of the charge density of states $\rho_{\text{CDOS}}^i = \sum_{\sigma} (|u_{i\sigma}|^2 - |v_{i\sigma}|^2)$ corresponding to the lowest positive-energy eigenstate at $\mu = 0.5$ meV. The profiles of ρ_{LDOS}^i and ρ_{CDOS}^i , at $\mu = -0.5$ meV where the JJ is in the topologically-trivial superconducting regime, are shown in Fig. 2f and Fig. 2g, respectively. In this case, both the quasiparticle state and the charge density are distributed near the middle of the quasi-one-dimensional channel. Interestingly, a comparison of Fig. 2e and Fig. 2g, implies an order-of-magnitude suppression in ρ_{CDOS}^i which is reminiscent of the local charge-neutrality signature of the MBS and is another confirmation of the Majorana character of this state. The above results establish that the SOC, generated by the SkX, alone can lead to the emergence of the MBS in the planar JJ devices.

The skyrmion size in a SkX is tunable, with remark-

able precession, by an external magnetic field, magnetic anisotropy and advanced symmetry protocol at heterointerfaces³⁰⁻³². In our Monte Carlo simulations, the skyrmion size was varied by tuning the magnetic field and the DMI, as shown in Figs. 3a-c. The Bogoliubov-de Gennes quasiparticle spectra at different skyrmion sizes, shown in Figs. 3d-f, imply that the presence of the zero energy MBS at a given chemical potential can be turned ON or OFF by only changing the skyrmion properties. The minimum diameter of the skyrmions, realized in our Monte Carlo simulations, is 10 lattice spacings for which the MBS appear in the discussed planar JJ setting. With increasing the skyrmion size, we find that the range of the chemical potential within which the MBS appear decreases effectively, however, the oscillation amplitude of the MBS is suppressed gradually. Therefore, the skyrmions offer a unique ability to manipulate the localization length of the MBS in the planar JJs. The strongly-localized MBS in the skyrmion-tuned planar JJs can, therefore, have advantageous over other platforms for MBS realization in fault-tolerant topological quantum computing. The MBS remain robust in the presence of the intrinsic Rashba SOC that exists in semiconductor-superconductor interfaces (Supplementary Information SIII).

Another important control parameter, that sets the

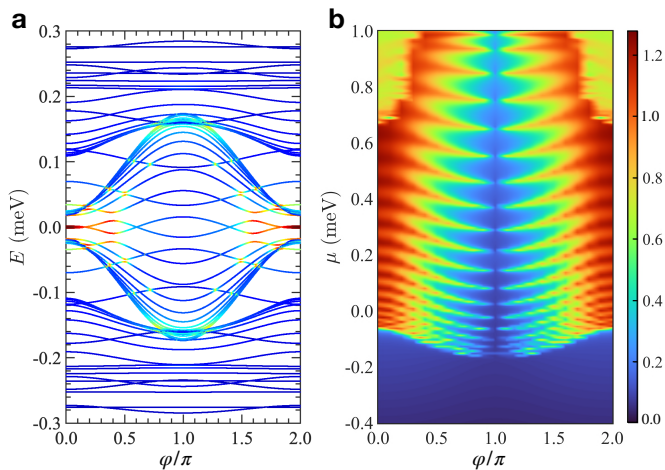


FIG. 4. **Phase tuning of the Majorana bound states.** **a.** Quasiparticle spectrum of the planar Josephson junction at a chemical potential $\mu = 0.5$ meV with changing phase difference φ between the two superconducting regions. The skyrmion diameter of the skyrmion crystal was $D_{sk} = 10a$. **b.** Colormap of the Majorana polarization of the lowest positive energy state in the plane spanned by the phase difference φ and the chemical potential μ . The Majorana bound states appear in the parameter regimes with $\mathcal{P}_M \geq 1$, $\varphi = 0$ being the most favorable scenario in this set up.

planar JJs apart from other platforms hosting the MBS, is the phase difference φ between the two superconducting regions of a JJ. The theoretical prediction¹³ and the subsequent experimental discoveries^{14,15} suggest that the JJ needs to be biased by a phase difference $\varphi = \pi$ to minimize the critical Zeeman field, required for inducing the topological superconductivity. Remarkably, in the current JJ set up with the SkX, the topological superconductivity is induced at $\varphi = 0$, as depicted by the quasiparticle spectrum with varying φ in Fig. 4a. With increasing φ , the MBS move gradually from zero to higher energies, indicating an enhancement in the localization length of the MBS. The MBS appear again at zero energy above $\varphi \approx 3\pi/2$. This dephasing effect of the MBS can be further understood from the Majorana oscillations – as we find that the oscillation increases with increasing φ in the range $0 < \varphi \leq \pi$ (Supplementary Information SII). The middle metallic region of the JJ can be perceived as a quasi-one-dimensional void region surrounded by the superconducting 2DEG. Additional phase difference between the two superconducting sides, therefore, only causes disruption to the induced topological superconductivity. This phenomenon generically takes place at several values of the chemical potential, as shown in Fig. 4b, where we plot the Majorana polarization \mathcal{P}_M of the lowest positive energy eigenstate in the parameter space spanned by the phase difference φ and the chemical potential μ . For the chosen range of μ values, the Majorana polarization decreases substantially within the range $\pi/2 \lesssim \varphi \lesssim 3\pi/2$. The Majorana oscillation in \mathcal{P}_M , however, survives up to $\varphi \approx \pi$. At $\varphi = \pi$, \mathcal{P}_M

vanishes completely, indicating the disappearance of the MBS. Therefore, $\varphi = 0$ is the most favorable condition to realize the MBS in our JJ set up and the phase difference can be further tuned to control the presence of the MBS.

The skyrmions bring outstanding control functionalities to the planar JJs for the creation and manipulation of the zero-energy MBS and their localization properties. The SkXs, being realized in an abundance of magnetic materials and also artificially created in patterned magnetic materials, offer a novel, feasible approach for advanced manipulation of the zero-energy MBS. The proposed planar JJ, combined with a SkX, has the major advantages that there is no need for a strong intrinsic Rashba-type SOC and phase-biasing constraint for the realization of the zero-energy MBS. The enhanced tunability of the MBS in the proposed two-dimensional platform opens up opportunities for designing new MBS braiding protocols for the fault-tolerant topological quantum computing, and investigating Majorana spectroscopy using the multi-terminal superconducting quantum interference devices.

Acknowledgements

This work was supported by the U.S. Department of Energy (DOE), Office of Science, Basic Energy Sciences (BES), Materials Sciences and Engineering Division.

REFERENCES

- ¹ A.Yu. Kitaev, “Fault-tolerant quantum computation by anyons,” *Ann. Phys.* **303**, 2 (2003).
- ² M. M. Desjardins, L. C. Contamin, M. R. Delbecq, M. C. Dartiailh, L. E. Bruhat, T. Cubaynes, J. J. Viennot, F. Mallet, S. Rohart, A. Thiaville, A. Cottet, and T. Kontos, “Synthetic spin-orbit interaction for Majorana devices,” *Nat. Mater.* **18**, 1060–1064 (2019).
- ³ A. Yazdani, “Conjuring Majorana with synthetic magnetism,” *Nat. Mater.* **18**, 1036 (2019).
- ⁴ C. Nayak, S. H. Simon, A. Stern, M. Freedman, and S. Das Sarma, “Non-abelian anyons and topological quantum computation,” *Rev. Mod. Phys.* **80**, 1083–1159 (2008).
- ⁵ J. Alicea, Y. Oreg, G. Refael, F. von Oppen, and M. P. A. Fisher, “Non-Abelian statistics and topological quantum information processing in 1D wire networks,” *Nat. Phys.* **7**, 412 (2011).
- ⁶ M. Kjaergaard, K. Wölms, and K. Flensberg, “Majorana fermions in superconducting nanowires without spin-orbit coupling,” *Phys. Rev. B* **85**, 020503 (2012).
- ⁷ J. Klinovaja, P. Stano, A. Yazdani, and D. Loss, “Topological superconductivity and Majorana fermions in RKKY systems,” *Phys. Rev. Lett.* **111**, 186805 (2013).
- ⁸ N. Mohanta, T. Zhou, J.-W. Xu, J. E. Han, A. D. Kent, J. Shabani, I. Žutić, and Alex Matos-Abiague, “Electrical Control of Majorana Bound States Using Magnetic Stripes,” *Phys. Rev. Applied* **12**, 034048 (2019).
- ⁹ T. Zhou, N. Mohanta, J. E. Han, A. Matos-Abiague, and I. Žutić, “Tunable magnetic textures in spin valves: From spintronics to Majorana bound states,” *Phys. Rev. B* **99**, 134505 (2019).

- ¹⁰ J. Herbrych, M. Środa, G. Alvarez, M. Mierzejewski, and E. Dagotto, “Interaction-induced topological phase transition and Majorana edge states in low-dimensional orbital-selective Mott insulators,” arXiv:2011.05646 (2020).
- ¹¹ J. Shabani, M. Kjaergaard, H. J. Suominen, Younghyun Kim, F. Nichele, K. Pakrouski, T. Stankevic, R. M. Lutchyn, P. Krogstrup, R. Feidenhans’l, S. Kraemer, C. Nayak, M. Troyer, C. M. Marcus, and C. J. Palmstrøm, “Two-dimensional epitaxial superconductor-semiconductor heterostructures: A platform for topological superconducting networks,” *Phys. Rev. B* **93**, 155402 (2016).
- ¹² T. Karzig, C. Knapp, R. M. Lutchyn, P. Bonderson, M. B. Hastings, C. Nayak, J. Alicea, K. Flensberg, S. Plugge, Y. Oreg, C. M. Marcus, and M. H. Freedman, “Scalable designs for quasiparticle-poisoning-protected topological quantum computation with Majorana zero modes,” *Phys. Rev. B* **95**, 235305 (2017).
- ¹³ F. Pientka, A. Keselman, E. Berg, A. Yacoby, A. Stern, and B. I. Halperin, “Topological Superconductivity in a Planar Josephson Junction,” *Phys. Rev. X* **7**, 021032 (2017).
- ¹⁴ H. Ren, F. Pientka, S. Hart, A. T. Pierce, M. Kosowsky, L. Lunczer, R. Schlereth, B. Scharf, E. M. Hankiewicz, L. W. Molenkamp, B. I. Halperin, and A. Yacoby, “Topological superconductivity in a phase-controlled Josephson junction,” *Nature* **569**, 93 (2019).
- ¹⁵ A. Fornieri, A. M. Whiticar, F. Setiawan, E. Portolés, A. C. C. Drachmann, A. Keselman, S. Gronin, C. Thomas, T. Wang, R. Kallaher, G. C. Gardner, E. Berg, M. J. Manfra, A. Stern, C. M. Marcus, and F. Nichele, “Evidence of topological superconductivity in planar Josephson junctions,” *Nature* **569**, 89 (2019).
- ¹⁶ E. Mascot, J. Bedow, M. Graham, S. Rachel, and D. K. Morr, “Topological Superconductivity in Skyrmion Lattices,” arXiv:2005.00027 (2020).
- ¹⁷ J. Bedow, E. Mascot, T. Posske, G. S. Uhrig, R. Wiesendanger, S. Rachel, and D. K. Morr, “Topological superconductivity induced by a triple-q magnetic structure,” *Phys. Rev. B* **102**, 180504 (2020).
- ¹⁸ N. Mohanta, E. Dagotto, and S. Okamoto, “Topological Hall effect and emergent skyrmion crystal at manganite-iridate oxide interfaces,” *Phys. Rev. B* **100**, 064429 (2019).
- ¹⁹ U. K. Rößler, A. N. Bogdanov, and C. Pfleiderer, “Spontaneous skyrmion ground states in magnetic metals,” *Nature* **442**, 797 (2006).
- ²⁰ S. Mühlbauer, B. Binz, F. Jonietz, C. Pfleiderer, A. Rosch, A. Neubauer, R. Georgii, and P. Böni, “Skyrmion lattice in a chiral magnet,” *Science* **323**, 915 (2009).
- ²¹ X. Z. Yu, Y. Onose, N. Kanazawa, J. H. Park, J. H. Han, Y. Matsui, N. Nagaosa, and Y. Tokura, “Real-space observation of a two-dimensional skyrmion crystal,” *Nature* **465**, 901 (2010).
- ²² L. Sun, R. X. Cao, B. F. Miao, Z. Feng, B. You, D. Wu, W. Zhang, An Hu, and H. F. Ding, “Creating an artificial two-dimensional Skyrmion crystal by nanopatterning,” *Phys. Rev. Lett.* **110**, 167201 (2013).
- ²³ Ö. Gül, H. Zhang, F. K. de Vries, J. van Veen, K. Zuo, V. Mourik, S. Conesa-Boj, M. P. Nowak, D. J. van Woerkom, M. Quintero-Pérez, M. C. Cassidy, A. Geresdi, S. Koelling, D. Car, S. R. Plissard, E. P. A. M. Bakkers, and L. P. Kouwenhoven, “Hard Superconducting Gap in InSb Nanowires,” *Nano Lett.* **17**, 2690 (2017).
- ²⁴ M. T. Deng, S. Vaitiekėnas, E. B. Hansen, J. Danon, M. Leijnse, K. Flensberg, J. Nygård, P. Krogstrup, and C. M. Marcus, “Majorana bound state in a coupled quantum-dot hybrid-nanowire system,” *Science* **354**, 1557 (2016).
- ²⁵ B. Nedniyom, R. J. Nicholas, M. T. Emeny, L. Buckle, A. M. Gilbertson, P. D. Buckle, and T. Ashley, “Giant enhanced g-factors in an InSb two-dimensional gas,” *Phys. Rev. B* **80**, 125328 (2009).
- ²⁶ F. Qu, J. van Veen, F. K. de Vries, A. J. A. Beukman, M. Wimmer, W. Yi, A. A. Kiselev, B.-M. Nguyen, M. Sokolich, M. J. Manfra, F. Nichele, C. M. Marcus, and L. P. Kouwenhoven, “Quantized conductance and large g-factor anisotropy in InSb quantum point contacts,” *Nano Lett.* **16**, 7509 (2016).
- ²⁷ a is the lattice grid spacing used to discretize the kinetic energy term $\frac{p^2}{2m}$ within finite-difference approximation. It is immaterial as long as the lattice lengths remain fixed.
- ⁵ D. Sticlet, C. Bena, and P. Simon, “Spin and Majorana polarization in topological superconducting wires,” *Phys. Rev. Lett.* **108**, 096802 (2012).
- ⁷ B. Scharf, F. Pientka, H. Ren, A. Yacoby, and E. M. Hankiewicz, “Tuning topological superconductivity in phase-controlled Josephson junctions with Rashba and Dresselhaus spin-orbit coupling,” *Phys. Rev. B* **99**, 214503 (2019).
- ³⁰ A. Soumyanarayanan, M. Raju, A. L. Gonzalez Oyarce, Anthony K. C. Tan, M.-Y. Im, A. P. Petrović, Pin Ho, K. H. Khoo, M. Tran, C. K. Gan, F. Ernult, and C. Panagopoulos, “Tunable room-temperature magnetic Skyrmions in Ir/Fe/Co/Pt multilayers,” *Nat. Mater.* **16**, 898 (2017).
- ³¹ E. Skoropata, J. Nichols, J. M. Ok, R. V. Chopdekar, E. S. Choi, A. Rastogi, C. Sohn, X. Gao, S. Yoon, T. Farmer, R. D. Desautels, Y. Choi, D. Haskel, J. W. Freeland, S. Okamoto, M. Brahlek, and H. N. Lee, “Interfacial tuning of chiral magnetic interactions for large topological Hall effects in LaMnO₃/SrIrO₃ heterostructures,” *Sci. Adv.* **6**, eaaz3902 (2020).
- ³² R. Lo Conte, A. K. Nandy, G. Chen, A. L. Fernandes Cauduro, A. Maity, C. Ophus, Z. Chen, A. T. N’Diaye, K. Liu, A. K. Schmid, and R. Wiesendanger, “Tuning the properties of zero-field room temperature ferromagnetic Skyrmions by interlayer exchange coupling,” *Nano Lett.* **20**, 4739 (2020).

Supplementary Information

Contents:

SI. Methods of calculations

SII. Majorana oscillations in the Josephson junctions

SIII. Effect of the intrinsic Rashba spin-orbit coupling

SIV. Characteristics of the Majorana bound states

SI. Methods of calculations

1. Monte Carlo simulations. The SkX spin configurations were obtained using a $L_x \times L_y \times L_z$ lattice with periodic boundary conditions along the x and y directions and open boundary conditions along the z direction. A bias-free sampling method, that provides a full and uniform coverage of the phase space spanned by the spin angles, was used for generating the completely random spin configurations. The calculation was started at a high temperature $T = 10J$ with a random spin configuration and the temperature was lowered slowly down to a low value $T = 0.001J$ in 2000 steps. At each temperature step, 10^{10} Monte Carlo spin updates were performed. In each spin update step, a new spin direction was chosen randomly within a small cone spanned around the initial spin direction^{1,2}. The new spin configuration was accepted or rejected according to the Metropolis energy-minimization algorithm by comparing the total energies of the previous and the new trial spin configurations, calculated using the Hamiltonian (1) of the main text.

2. Self-consistent Bogoliubov-de Gennes formalism.

The Hamiltonian (2) of the main text, which is quadratic in the fermionic operators $\hat{c}_{i\sigma}$, can be solved by exact diagonalization via a unitary transformation

$$\hat{c}_{i\sigma} = \sum_n u_{i\sigma}^n \hat{\gamma}_n + v_{i\sigma}^{n*} \hat{\gamma}_n^\dagger, \quad (\text{E1})$$

where $\hat{\gamma}_n^\dagger$ ($\hat{\gamma}_n$) is a fermionic creation (annihilation) operator of the quasiparticle/quasihole state in the n^{th} energy eigenstate. The quasiparticle amplitudes $u_{i\sigma}^n$ and the quasihole amplitudes $v_{i\sigma}^n$ are determined by solving the Bogoliubov-de Gennes (BdG) equations: $\sum_j \mathcal{H}_{ij} \psi_j^n = \epsilon_n \psi_n^n$, where $\psi_n^n = [u_{i\uparrow}^n, u_{i\downarrow}^n, v_{i\uparrow}^n, v_{i\downarrow}^n]^T$ is the BdG basis wave function and ϵ_n is the n^{th} energy eigenvalue. The Hamiltonian \mathcal{H}_{ij} is expressed in the following matrix form

$$\mathcal{H}_{ij} = \begin{pmatrix} \mathcal{H}_{\uparrow\uparrow} & \mathcal{H}_{\uparrow\downarrow} & 0 & \Delta_i \\ \mathcal{H}_{\downarrow\uparrow} & \mathcal{H}_{\downarrow\downarrow} & -\Delta_i & 0 \\ 0 & -\Delta_i^* & -\mathcal{H}_{\uparrow\uparrow}^* & -\mathcal{H}_{\uparrow\downarrow}^* \\ \Delta_i^* & 0 & -\mathcal{H}_{\downarrow\uparrow}^* & -\mathcal{H}_{\downarrow\downarrow}^* \end{pmatrix}, \quad (\text{E2})$$

where $\mathcal{H}_{\uparrow\uparrow, \downarrow\downarrow} = -t(1 - \delta_{ij}) + (4t - \mu)\delta_{ij} - 1/2\sigma g\mu_B B_z$, where $\sigma = \pm$ for $\uparrow\uparrow, \downarrow\downarrow$, and $\mathcal{H}_{\uparrow\downarrow} = -1/2g\mu_B(B_x + iB_y)$. The s -wave pairing amplitude $\Delta_i = -U_i \langle c_{i\uparrow} c_{i\downarrow} \rangle$ is computed using

$$\Delta_i = -U \sum_n [u_{i\uparrow}^n v_{i\downarrow}^{n*} (1 - f(\epsilon_n)) + u_{i\downarrow}^n v_{i\uparrow}^{n*} f(\epsilon_n)], \quad (\text{E3})$$

where $U_i = U$ inside the two superconducting regions and zero in the middle quasi-one-dimensional metallic channel, $f(\epsilon_n) = 1/(1 + e^{\epsilon_n/k_B T})$ is the Fermi-Dirac distribution function at temperature T . The self-consistency iterations were performed until the pairing amplitudes Δ_i are converged

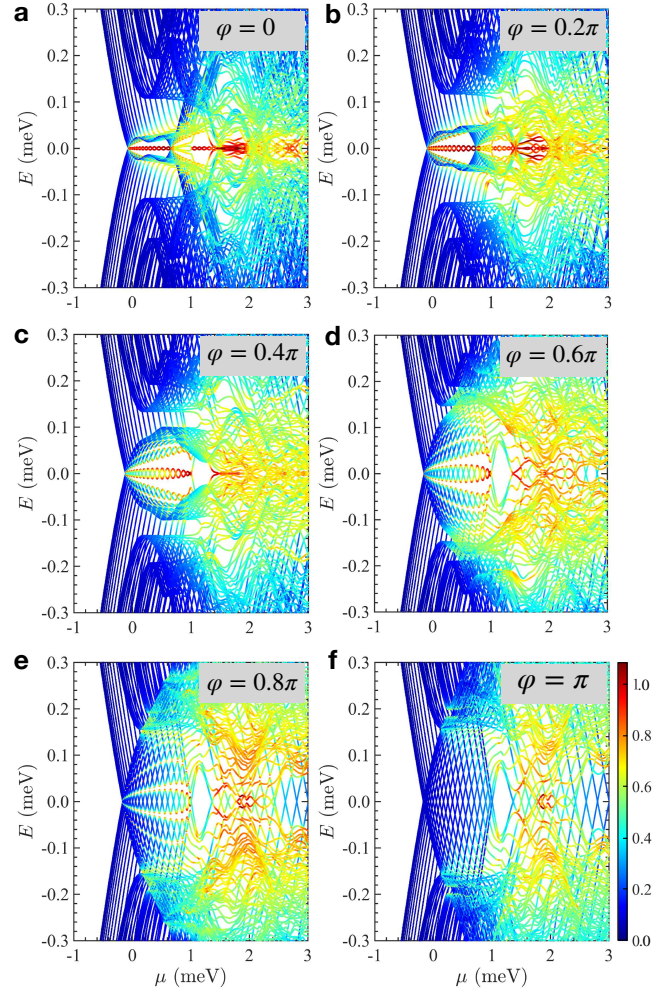


FIG. S1. Quasiparticle spectrum of a planar Josephson junction, attached to a skyrmion crystal as considered in Fig.2 of the main text, with varying chemical potential μ at different values of the phase difference φ between the two superconducting regions of the Josephson junction. The colorbar represents, in arbitrary units, the Majorana polarization \mathcal{P}_M . The intrinsic Rashba spin-orbit coupling is set to zero. All other parameters are as in the Fig.2 of the main text.

at every lattice sites.

SII. Majorana oscillations in the Josephson junctions

The oscillation of the Majorana bound states (MBS) is a well-known phenomenon that appears due to the finite size effect. In a one-dimensional geometry, *e.g.* a Rashba nanowire with a Zeeman exchange coupling, the probability density of the MBS, which are localized dominantly at the two ends, decay exponentially with distance towards the middle of the nanowire. The overlap of these two MBS wave functions give rise to a finite splitting in energy. This split energy gap between the MBS pair oscillates with varying a parameter, such as the chemical potential or the Zeeman energy. In our considered planar Josephson junction (JJ) geometry, the finite length of the quasi-one-dimensional

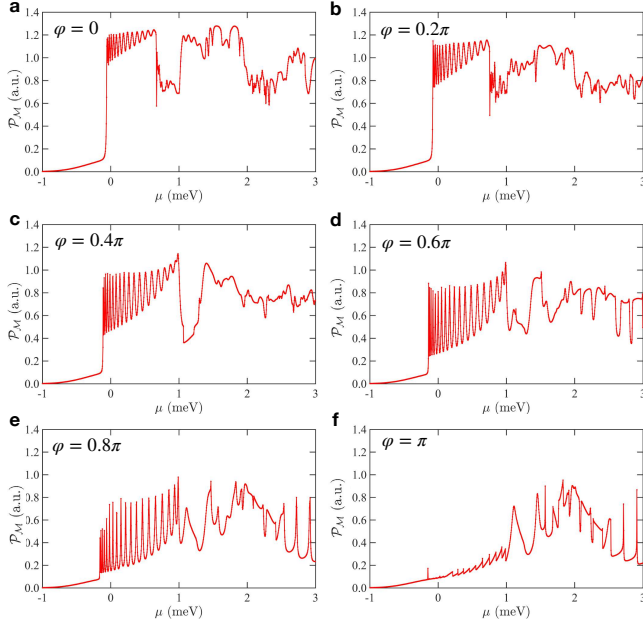


FIG. S2. The Majorana polarization \mathcal{P}_M of the lowest positive energy eigenstate with varying chemical potential μ at different values of the phase difference φ . The intrinsic Rashba spin-orbit coupling is kept at zero. All other parameters are as in the Fig.2 of the main text.

metallic channel in the middle, therefore, naturally leads to the oscillations of the zero-energy MBS with varying chemical potential μ . Furthermore, the finite width of the quasi-one-dimensional channel provides extra room for delocalization of the MBS at the two ends, contributing additively to the Majorana oscillation. The oscillation amplitude, however, decreases with increasing the length of the JJ. In Fig. S1, we show the quasiparticle spectra with varying μ at different values of the phase difference φ between the two superconducting regions of the JJ. Evidently, the oscillation amplitude increases with increasing φ from 0 to π . At $\varphi = \pi$, the oscillation becomes large and the MBS completely vanish. The oscillation can also be visible in the Majorana polarization \mathcal{P}_M . In Fig. S2, we show the variation in \mathcal{P}_M for the lowest positive eigenstate with μ . At $\varphi = 0$, the oscillation is small in amplitude and appears on the top of a significant value of the Majorana polarization ($\mathcal{P}_M \geq 1$). With increasing φ from 0 to π , the value of \mathcal{P}_M decreases and the oscillation amplitude increases simultaneously. These results explain why the MBS disappear with increasing the phase difference φ from 0 to π , as discussed in the main text.

III. Effect of the intrinsic Rashba spin-orbit coupling

The broken inversion symmetry at the interface between the two-dimensional electron gas and the superconductor, often leads to a sizable intrinsic Rashba spin-orbit coupling (SOC) which is usually considered as the primary mechanism for modifying the pairing symmetry of the induced superconductivity in a one-dimensional³ or two-dimensional geometry⁴, leading to the desired topological superconductivity. To explore the mutual influence of the Rashba SOC and the SkX-generated SOC on the emergence of the zero-energy MBS, we consider the

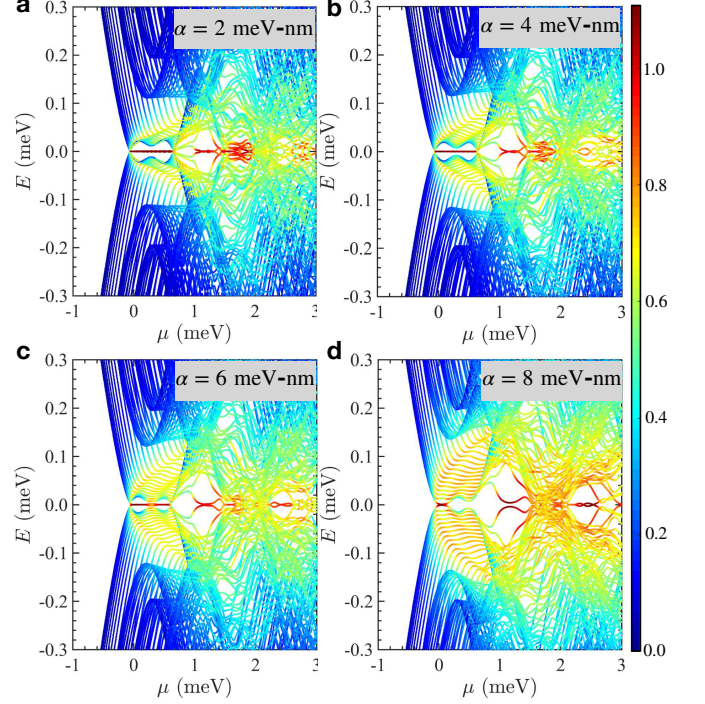


FIG. S3. Quasiparticle spectrum of the planar Josephson junction as considered in Fig.2 of the main text at phase difference $\varphi = 0$ with varying chemical potential at different values of the intrinsic Rashba spin-orbit coupling: **a.** $\alpha = 2$ meV-nm, **b.** $\alpha = 4$ meV-nm, **c.** $\alpha = 6$ meV-nm, and **d.** $\alpha = 8$ meV-nm. The colorbar represents the Majorana polarization \mathcal{P}_M , in arbitrary units. The Majorana bound states remain robust in the presence of the intrinsic Rashba spin-orbit coupling.

Hamiltonian $\mathcal{H}_{\text{RSOC}} = -i\alpha/(2a) \sum_{\langle ij \rangle, \sigma, \sigma'} (\boldsymbol{\sigma} \times \hat{r}_{ij})^z_{\sigma\sigma'} c_{i\sigma}^\dagger c_{j\sigma'}$ for the Rashba SOC, where α is the strength of the Rashba SOC, and obtain the quasiparticle spectrum based on the total Hamiltonian $\mathcal{H}_{\text{BdG}} + \mathcal{H}_{\text{RSOC}}$. In Fig. S4, we show the quasiparticle spectra for four different values of α . With relatively smaller values of α , e.g. **a.** $\alpha = 2$ meV-nm and **b.** $\alpha = 4$ meV-nm, the zero-energy MBS within the range -0.2 meV $\lesssim \mu \lesssim 0.6$ meV, remain stable. The oscillations of the MBS are minimized within this range of μ , making the MBS more robust (*i.e.* localized). For larger values of α (cases **c.** and **d.**), the MBS in the above range of μ start to become delocalized, possibly because a very large Rashba SOC interferes destructively with the synthetic SOC. But remarkably, with larger values of α , new MBS start to appear at larger values of the chemical potential, e.g. within the range 2.2 meV $\lesssim \mu \lesssim 2.6$ meV. Although the mutual effects of the intrinsic Rashba SOC and the SkX-generated SOC are rather complex, within some ranges of μ , they cooperate to generate robust MBS with a larger topological energy gap.

SIV. Characteristics of the Majorana bound states

To characterize the MBS in a one-dimensional system, the Majorana number or the Winding number is usually computed. However, it is not feasible to calculate this topological invariant in a quasi-one dimensional system that lacks

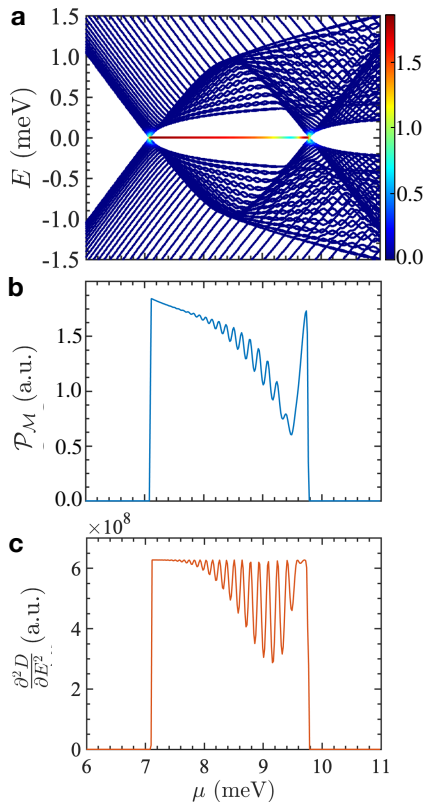


FIG. S4. **a.** Quasiparticle spectrum, with varying chemical potential μ , of a wire of length $L_x = 190a$ (a being the unit lattice spacing) that is placed at the middle of a superconductor of size $200a \times 5a$. A Zeeman field $B = 0.3$ T is uniformly present throughout the wire. The Rashba spin-orbit coupling strength is $\alpha = 30$ meV-nm. The g-factor is $g = 200$. The superconducting potential is $U = 2$ meV and the pairing amplitude Δ_i is treated self-consistently. The colorbar represents the Majorana polarization \mathcal{P}_M in arbitrary units. **b.** The μ variation of \mathcal{P}_M of the lowest positive energy eigenstate. **c.** The μ variation of $\frac{\partial^2 D}{\partial E^2}$, the curvature of the density of states at zero energy in arbitrary units.

the translational symmetry. Therefore, in our platform, to identify the MBS in the quasiparticle spectrum and track the transition to the topological superconducting phase, we calculate primarily two quantities: (i) the generalized Majorana polarization \mathcal{P}_M , proposed in Refs. 5 and 6, and (ii) the second derivative of the total density of states at zero energy, $\frac{\partial^2 D}{\partial E^2}$ which can also be called the curvature of the density of states. The second derivative of the local density of states at a boundary site and at zero energy was used as an order parameter in Ref. 7 to track the topological superconducting transition. These quantities may provide additional insight to detect the MBS in experiments, besides the conventional

zero-bias conductance peak⁸ which often leads to ambiguity due to other possible zero-bias states in a superconductor⁹. To test the above two quantities in our set up, we first consider a chain with Rashba SOC and a uniform Zeeman exchange coupling, attached on the top and at the middle of a quasi-one-dimensional s -wave superconductor. The BdG quasiparticle spectrum of such a system, shown in Fig. S4a, depicts the emergence of the zero-energy MBS within a range of the chemical potential μ . The μ -variation of the two above-discussed quantities, \mathcal{P}_M and $\frac{\partial^2 D}{\partial E^2}$, are plotted in, respectively, Fig. S4b and c. Interestingly, both these quantities reveal sharp jumps on entering the topological superconducting phase, similar to an order parameter in an ordinary phase transition. The Majorana oscillations, although not noticeable in the quasiparticle spectrum, is visible in both \mathcal{P}_M and $\frac{\partial^2 D}{\partial E^2}$. In the infinite-length limit, the Majorana oscillations vanish and both these quantities reveal a quantized feature, as shown previously in Ref. 5. The sharp jumps, therefore, attest that these two quantities can reliably be used to track the topological superconducting transition in our computational framework.

REFERENCES

- ¹ N. Mohanta, S. Okamoto, and E. Dagotto, “Planar topological Hall effect from conical spin spirals,” *Phys. Rev. B* **102**, 064430 (2020).
- ² N. Mohanta, A. D. Christianson, S. Okamoto, and E. Dagotto, “Signatures of a liquid-crystal transition in spin-wave excitations of skyrmions,” *Commun. Phys.* **3**, 229 (2020).
- ³ N. Mohanta and A. Taraphder, “Topological superconductivity and Majorana bound states at the LaAlO₃/SrTiO₃ interface,” *EPL (Europhysics Letters)* **108**, 60001 (2014).
- ⁴ N. Mohanta, A. P. Kampf, and T. Kopp, “Supercurrent as a probe for topological superconductivity in magnetic adatom chains,” *Phys. Rev. B* **97**, 214507 (2018).
- ⁵ D. Sticlet, C. Bena, and P. Simon, “Spin and Majorana polarization in topological superconducting wires,” *Phys. Rev. Lett.* **108**, 096802 (2012).
- ⁶ N. Sedlmayr and C. Bena, “Visualizing Majorana bound states in one and two dimensions using the generalized Majorana polarization,” *Phys. Rev. B* **92**, 115115 (2015).
- ⁷ B. Scharf, F. Pientka, H. Ren, A. Yacoby, and E. M. Hankiewicz, “Tuning topological superconductivity in phase-controlled Josephson junctions with Rashba and Dresselhaus spin-orbit coupling,” *Phys. Rev. B* **99**, 214503 (2019).
- ⁸ K. Sengupta, I. Žutić, H.-J. Kwon, V. M. Yakovenko, and S. Das Sarma, “Midgap edge states and pairing symmetry of quasi-one-dimensional organic superconductors,” *Phys. Rev. B* **63**, 144531 (2001).
- ⁹ L. Kuerten, C. Richter, N. Mohanta, T. Kopp, A. Kampf, J. Mannhart, and H. Boschker, “In-gap states in superconducting LaAlO₃/SrTiO₃ interfaces observed by tunneling spectroscopy,” *Phys. Rev. B* **96**, 014513 (2017).